Test functions for three-dimensional control-volume mixed finite-element methods on irregular grids

R.L. Naff
U.S. Geological Survey, Denver, CO USA

T.F. Russell and J.D. Wilson
University of Colorado at Denver, Denver, CO USA

ABSTRACT: Numerical methods based on unstructured grids, with irregular cells, usually require discrete shape functions to approximate the distribution of quantities across cells. For control-volume mixed finite-element methods, vector shape functions are used to approximate the distribution of velocities across cells and vector test functions are used to minimize the error associated with the numerical approximation scheme. For a logically cubic mesh, the lowest-order shape functions are chosen in a natural way to conserve intercell fluxes that vary linearly in logical space. Vector test functions, while somewhat restricted by the mapping into the logical reference cube, admit a wider class of possibilities. Ideally, an error minimization procedure to select the test function from an acceptable class of candidates would be the best procedure. Lacking such a procedure, we first investigate the effect of possible test functions on the pressure distribution over the control volume; specifically, we look for test functions that allow for the elimination of intermediate pressures on cell faces. From these results, we select three forms for the test function for use in a control-volume mixed method code and subject them to an error analysis for different forms of grid irregularity; errors are reported in terms of the discrete L^2 norm of the velocity error. Of these three forms, one appears to produce optimal results for most forms of grid irregularity.

1 INTRODUCTION

For simulation of two-dimensional (2-D) flow in heterogeneous porous media, it has been shown that mixed methods, and in particular the control-volume mixed finite-element (CVMFE) methods, are often the most efficient methods for solving for the velocity field (e.g., Durlofsky (1994), Cai et al. (1997)). In this report, three different test functions are evaluated for use in the the CVMFE method. The performance of the test functions is evaluated using the L^2 norm of the velocity error from a number of test cases. The three-dimensional (3-D) algorithm described herein is based on the CVMFE methodology as developed by Cai et al. (1997) for the simulation of Darcian flow in two dimensions. In the process of extending the CVMFE methodology to three dimensions, some of the deficiencies in the work by Cai et al. (1997) were investigated, which led us to believe that a different test function might improve the performance of the method. In addition, it has been discovered that the vector shape functions used in this original investigation do not scale up to three dimensions as well as we had hoped. While this latter problem is still under investigation, it is noteworthy as it also affects the interpretation of these L^2 results.

In the CVMFE method, the domain is discretized into potentially irregular hexahedral cells; that the cells can have irregular shapes allows for the modeling of complex hydrogeological systems. Vector shape functions, as described subsequently, serve as basis functions to interpolate the velocity over the interior of cells. Vector test functions, on the other hand, are used as weighting factors for integrating the Darcy relation over control volumes associated with cell faces; this usage can be viewed as an error minimization step in the control volume technique. As developed for CVMFE methods, an additional requirement is placed on the test functions in that their use is expected to facilitate the elimination of pressures on faces between cells; these pressures are extraneous to the mixed-method algorithm. Our intent is to develop the CVMFE method for the simulation of flow in 3-D heterogeneous media.

In the subsequent three sections of this report, background information concerning the nature of the problem being solved and the solution technique are discussed. In particular, in section 3 the vector shape functions used in this study are presented, and in section 4 the rationale for the three test functions is detailed. The first test problem, for uniform flow

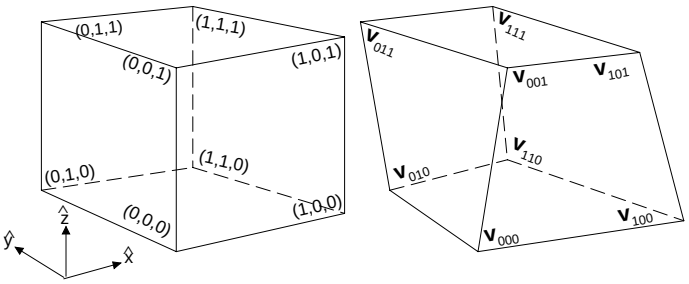

Figure 1: Left: reference cube $\hat{Q}$ with edges of unit length. Right: arbitrary cell Q from discretization with vertex locations $\mathbf{v}_{000}$, $\mathbf{v}_{100}$, $\mathbf{v}_{010}$, $\mathbf{v}_{001}$, $\mathbf{v}_{110}$, $\mathbf{v}_{101}$, $\mathbf{v}_{011}$ and $\mathbf{v}_{111}$ indicated.

in a simply distorted three-dimensional domain, follows in section 5. In section 6, a two-dimensional nonuniform flow problem is presented for which an analytical solution exists. A brief discussion of the results concludes the report. The discussion of the CVMFE method presented herein is necessarily brief; the reader is invited to examine the work by Cai et al. (1997) for a complete explanation of the 2-D algorithm.

The algorithm used in this study is strictly three dimensional; when 2-D simulations were desired, a grid was constructed from a single layer of cells of uniform thickness such that the surface of this layer gives the desired 2-D grid. When the correct test function is used, this procedure results in matrix equations that are identical to those resulting from the 2-D algorithm of Cai et al. (1997). Thus, the 2-D simulation presented herein has all the characteristics of simulation from a strictly 2-D algorithm.

2 BASIC EQUATIONS

The numerical method outlined in this paper is based on the following steady flow equation applied within a 3-D domain Ω:

$$\nabla \cdot \mathbf{q} \;=\; W(x,y,z), \qquad (x,y,z) \in \Omega \tag{1}$$

Here $\mathbf{q}$ is the specific discharge vector and $W(x,y,z)$ is a source term. On the surface $\partial\Omega$ of the domain, boundary conditions can consist of fluxes over $\partial\Omega_f$ or specified pressures over $\partial\Omega_p$. The specific discharge $\mathbf{q}$ is defined from the Darcy relation:

$$\mathbf{q} \;=\; -\frac{\mathbf{K}(x,y,z)}{\mu}\nabla p \tag{2}$$

where p is the pressure, $\mathbf{K}(x,y,z)$ is the hydraulic conductivity tensor and μ is the viscosity (the gravitational potential is neglected from (2) for notational convenience). For the CVMFE method, the hydraulic conductivity tensor is inverted, causing (2) to be written as

$$\nabla p \;=\; -\mu\mathbf{K}^{-1}\mathbf{q} \tag{3}$$

The mixed-method development herein uses (1) and (3) as a basis of the numerical approximation.

The domain Ω is discretized using a logically regular mesh of hexahedral cells. These cells may be irregular in construction to the point where faces of the cells are not planar. Any given hexahedral cell Q can be described from the location of its vertices at $\mathbf{v}_{000}$, $\mathbf{v}_{100}$, $\mathbf{v}_{010}$, $\mathbf{v}_{001}$, $\mathbf{v}_{110}$, $\mathbf{v}_{101}$, $\mathbf{v}_{011}$ and $\mathbf{v}_{111}$, where $\mathbf{v}_{\alpha\beta\gamma} = (x_{\alpha\beta\gamma}, y_{\alpha\beta\gamma}, z_{\alpha\beta\gamma})$ (Figure 1). A trilinear mapping exists such that the hexahedral cell Q is the image of a regular reference hexahedron, $\hat{Q}$, consisting of unit cube with fixed vertices at $(0,0,0)$, $(1,0,0)$, $(0,1,0)$, $(0,0,1)$, $(1,1,0)$, $(1,0,1)$, $(0,1,1)$ and $(1,1,1)$ on a point by point basis; Figure 1 depicts these relations. This mapping allows that, for any reference location $\hat{\mathbf{r}} = (\hat{x},\hat{y},\hat{z})$ within $\hat{Q}$, the equivalent location $\mathbf{r} = (x,y,z)$ within Q is obtained from the following expression:

$$\begin{aligned}\mathbf{r} \;=\;& \mathbf{v}_o + \mathbf{v}_a\hat{x} + \mathbf{v}_b\hat{y} + \mathbf{v}_c\hat{z} + \mathbf{v}_d\hat{x}\hat{y} + \mathbf{v}_e\hat{x}\hat{z} + \mathbf{v}_f\hat{y}\hat{z} \\ &+ \mathbf{v}_g\hat{x}\hat{y}\hat{z}\end{aligned} \tag{4}$$

where $\mathbf{v}_o = \mathbf{v}_{000}$, $\mathbf{v}_a = \mathbf{v}_{100} - \mathbf{v}_o$, $\mathbf{v}_b = \mathbf{v}_{010} - \mathbf{v}_o$, $\mathbf{v}_c = \mathbf{v}_{001} - \mathbf{v}_o$, $\mathbf{v}_d = \mathbf{v}_{110} - \mathbf{v}_o - \mathbf{v}_a - \mathbf{v}_b$, $\mathbf{v}_e = \mathbf{v}_{101} - \mathbf{v}_o - \mathbf{v}_a - \mathbf{v}_c$, $\mathbf{v}_f = \mathbf{v}_{011} - \mathbf{v}_o - \mathbf{v}_b - \mathbf{v}_c$, $\mathbf{v}_g = \mathbf{v}_{111} - \mathbf{v}_o - \mathbf{v}_a - \mathbf{v}_b - \mathbf{v}_c - \mathbf{v}_d - \mathbf{v}_e - \mathbf{v}_f$. This mapping is an extension of the conventional bilinear mapping for a logically rectangular grid (Cai et al. 1997; Garanzha & Konshin 1999). Note that, should $\hat{x}$ be fixed in $\hat{\mathbf{r}}$, then a face normal to $\hat{x}$ within $\hat{Q}$ is determined. This face is mapped, via (4), into an equivalent face within Q. Covariant vectors, defined as $\mathbf{X}(\hat{y},\hat{z}) \equiv \partial\mathbf{r}/\partial\hat{x}$, $\mathbf{Y}(\hat{x},\hat{z}) \equiv \partial\mathbf{r}/\partial\hat{y}$ and $\mathbf{Z}(\hat{x},\hat{y}) \equiv \partial\mathbf{r}/\partial\hat{z}$, allow for definition of the geometry of Q. The volumetric Jacobian J for passing from Q to $\hat{Q}$ is simply (Hildebrand 1962)

$$J(\hat{x},\hat{y},\hat{z}) \;=\; \mathbf{X}(\hat{y},\hat{z}) \cdot (\mathbf{Y}(\hat{x},\hat{z}) \times \mathbf{Z}(\hat{x},\hat{y})) \tag{5}$$

while, for a face in the logical x direction, the surface Jacobian Γ_x becomes (Hildebrand 1962)

$$\Gamma_x(\hat{x},\hat{y},\hat{z}) \;=\; |\mathbf{Y}(\hat{x},\hat{z}) \times \mathbf{Z}(\hat{x},\hat{y})| \tag{6}$$

Surface Jacobians can similarly be defined for faces in the logical y and z directions. These few relations allow us to define the necessary quantities used within the CVMFE method.

3 SHAPE FUNCTIONS

Velocity basis vectors $\mathbf{v}_{i,j,k;m,n,p}$ are associated with the bulk flux through each face of a cell $Q_{i,j,k}$; here i, j, k represents the location of a hexahedral cell within the discretized domain. The forms of the vector shape functions used in this study are

$$\mathbf{v}_{i,j,k;1/2,0,0} = \rho_{i+1/2,j,k}\frac{\hat{x}\mathbf{X}_{i,j,k}}{J_{i,j,k}} \quad (7a)$$

$$\mathbf{v}_{i,j,k;-1/2,0,0} = \rho_{i-1/2,j,k}\frac{(1-\hat{x})\mathbf{X}_{i,j,k}}{J_{i,j,k}} \quad (7b)$$

$$\mathbf{v}_{i,j,k;0,1/2,0} = \rho_{i,j+1/2,k}\frac{\hat{y}\mathbf{Y}_{i,j,k}}{J_{i,j,k}} \quad (7c)$$

$$\mathbf{v}_{i,j,k;0,-1/2,0} = \rho_{i,j-1/2,k}\frac{(1-\hat{y})\mathbf{Y}_{i,j,k}}{J_{i,j,k}} \quad (7d)$$

$$\mathbf{v}_{i,j,k;0,0,1/2} = \rho_{i,j,k+1/2}\frac{\hat{z}\mathbf{Z}_{i,j,k}}{J_{i,j,k}} \quad (7e)$$

$$\mathbf{v}_{i,j,k;0,0,-1/2} = \rho_{i,j,k-1/2}\frac{(1-\hat{z})\mathbf{Z}_{i,j,k}}{J_{i,j,k}} \quad (7f)$$

where $J_{i,j,k}$ is the volumetric Jacobian, $\mathbf{X}_{i,j,k}$, $\mathbf{Y}_{i,j,k}$ and $\mathbf{Z}_{i,j,k}$ are the covariant vectors for $Q_{i,j,k}$, and, for example, $\rho_{i+1/2,j,k}$ is an area correction factor for the face at $\hat{x} = 1$ (denoted as $F_{i+1/2,j,k}$) such that

$$\rho_{i+1/2,j,k}(\hat{y},\hat{z}) = \frac{\Gamma_{i+1/2,j,k}(\hat{y},\hat{z})}{A_{i+1/2,j,k}}$$

Here, $\Gamma_{i+1/2,j,k}(\hat{y},\hat{z}) = |\mathbf{Y}\times\mathbf{Z}|_{\hat{x}=1}$ is the surface Jacobian at $F_{i+1/2,j,k}$ and $A_{i+1/2,j,k}$ is the area of this face. Other area correction factors are expressed in a similar manner. These shape functions are an extension of those used by Cai et al. (1997) for simulation of flow in two dimensions. Using the velocity basis vectors, the specific discharge can be approximated at any point within a hexahedral cell $Q_{i,j,k}$ as

$$\begin{aligned}\mathbf{q} \approx\ & f_{i+1/2,j,k}\mathbf{v}_{i,j,k;1/2,0,0} + f_{i-1/2,j,k}\mathbf{v}_{i,j,k;-1/2,0,0} \\ & + f_{i,j+1/2,k}\mathbf{v}_{i,j,k;0,1/2,0} + f_{i,j-1/2,k}\mathbf{v}_{i,j-1/2,k;0,-1/2,0} \\ & + f_{i,j,k+1/2}\mathbf{v}_{i,j,k;0,0,1/2} + f_{i,j,k-1/2}\mathbf{v}_{i,j,k;0,0,-1/2} \quad (8)\end{aligned}$$

where, for example, $f_{i+1/2,j,k}$ is the bulk flux through face $F_{i+1/2,j,k}$. If this approximation is substituted into (1) and both sides are integrated over $Q_{i,j,k}$, then Gauss's divergence theorem implies that

$$\begin{aligned}& f_{i+1/2,j,k} - f_{i-1/2,j,k} + f_{i,j+1/2,k} - f_{i,j-1/2,k} \\ & + f_{i,j,k+1/2} - f_{i,j,k-1/2} = \int_{Q_{i,j,k}} W(x,y,z)\,dxdydz \quad (9)\end{aligned}$$

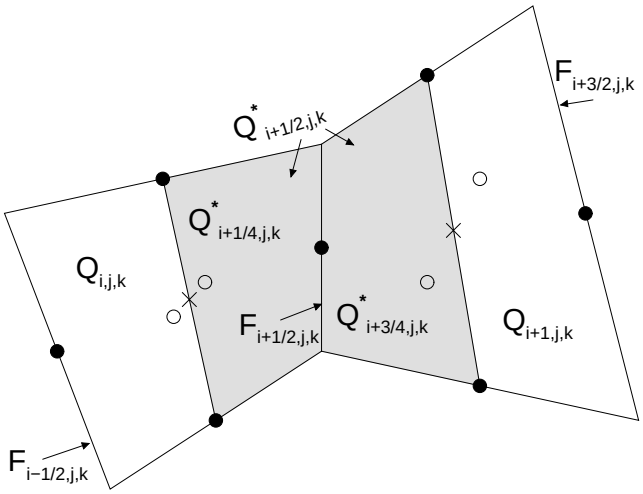

Figure 2: Midsection through two adjoining cells in the logical x direction. Filled and open circles represent locations on faces where fluxes are estimated; open circles represent flux locations on faces in the logical y direction projected onto midsection. The $\times$ symbol is used to denote pressure locations at logical cell centers.

Thus, the shape functions provide for a discrete form of the continuity equation within the discretized region Ω. While the above shape functions generally appear to provide an adequate representation of the specific discharge $\mathbf{q}$ over a cell in two dimensions, their use in three dimensions is more questionable. For the simulation of a uniform flow field in three dimensions with an irregular grid, it can be shown that these functions do not always properly capture the flux distribution across every irregular cell. This result may explain why, even with some very simple irregular grids, exact simulations of uniform flow are not achieved in three dimensions with the present CVMFE algorithm.

4 TEST FUNCTIONS

To develop a discrete form for the Darcy relation (3), a control volume which straddles a cell face within the discretized region Ω is used; a control volume $Q^*_{i+1/2,j,k}$ straddling $F_{i+1/2,j,k}$ is depicted in Figure 2. Weighted with a test function, the modified Darcy relation (3), with an approximation similar to (8) for the specific discharge, is integrated over a straddle control volume. The choice of the test function is motivated by the efficiency and convenience of eliminating intermediate pressures associated with faces adjoining two cells; in the logical x direction of Figure 2, this face is denoted as $F_{i+1/2,j,k}$. A simple form on which to base the test function in the logical x direction is the covariant vector $\mathbf{X}$; one form suggested by Cai et

al. (1997) for the test function is

$$\mathbf{w}_{i+1/2,j,k} = \begin{cases} \mathbf{X}_{i,j,k}/\Lambda_{i+1/4,j,k}, & \text{on } Q^*_{i+1/4,j,k} \\ \mathbf{X}_{i+1,j,k}/\Lambda_{i+3/4,j,k}, & \text{on } Q^*_{i+3/4,j,k} \\ 0, & \text{otherwise} \end{cases} \tag{10}$$

where

$$\Lambda_{i+1/4,j,k} = 2\int_0^1\int_0^1\int_{1/2}^1 J_{i,j,k}\,d\hat{x}d\hat{y}d\hat{z}$$

$$\Lambda_{i+3/4,j,k} = 2\int_0^1\int_0^1\int_0^{1/2} J_{i+1,j,k}\,d\hat{x}d\hat{y}d\hat{z}$$

This test function shall be referred to herein as the CJMR function. When applied to the left-hand side of (3), this test function gives the result

$$\begin{aligned}
&\int_{Q^*_{i+1/2,j,k}} \nabla p\cdot\mathbf{w}_{i+1/2,j,k}\,dxdydz \\
&= \frac{1}{\Lambda_{i+1/4,j,k}}\int_{Q^*_{i+1/4,j,k}} \nabla p\cdot\mathbf{X}_{i,j,k}\,dxdydz \\
&\quad + \frac{1}{\Lambda_{i+3/4,j,k}}\int_{Q^*_{i+3/4,j,k}} \nabla p\cdot\mathbf{X}_{i+1,j,k}\,dxdydz \\
&= \frac{1}{\Lambda_{i+1/4,j,k}}\int_{Q^*_{i+1/4,j,k}} \frac{\partial p}{\partial\hat{x}}\,dxdydz \\
&\quad + \frac{1}{\Lambda_{i+3/4,j,k}}\int_{Q^*_{i+3/4,j,k}} \frac{\partial p}{\partial\hat{x}}\,dxdydz \\
&= \frac{1}{\Lambda_{i+1/4,j,k}}\int_0^1\int_0^1\int_{1/2}^1 \frac{\partial p}{\partial\hat{x}}J_{i,j,k}\,d\hat{x}d\hat{y}d\hat{z} \\
&\quad + \frac{1}{\Lambda_{i+3/4,j,k}}\int_0^1\int_0^1\int_0^{1/2} \frac{\partial p}{\partial\hat{x}}J_{i+1,j,k}\,d\hat{x}d\hat{y}d\hat{z} \\
&\approx \frac{1}{2}\left[\left.\frac{\partial p}{\partial\hat{x}}\right|_{i+1/4,j,k} + \left.\frac{\partial p}{\partial\hat{x}}\right|_{i+3/4,j,k}\right] \\
&= p_{i+1,j,k} - p_{i,j,k}
\end{aligned} \tag{11}$$

which results by first assuming that the pressure varies linearly in reference space $\hat{Q}$ and then noting that this assumption implies

$$\left.\frac{\partial p}{\partial\hat{x}}\right|_{i+1/4,j,k} = 2(p_{i+1/2,j,k} - p_{i,j,k}), \quad (x,y,z)\in Q^*_{i+1/4,j,k}$$

$$\left.\frac{\partial p}{\partial\hat{x}}\right|_{i+3/4,j,k} = 2(p_{i+1,j,k} - p_{i+1/2,j,k}), \quad (x,y,z)\in Q^*_{i+3/4,j,k}$$

For an irregular grid, even in the presence of a uniform flow field, this assumption is unlikely to hold.

An alternate test function, which partially repairs this problem, is

$$\mathbf{w}^*_{i+1/2,j,k} = \begin{cases} \mathbf{X}_{i,j,k}/\Lambda^*_{i+1/4,j,k}, & \text{on } Q^*_{i+1/4,j,k} \\ \mathbf{X}_{i+1,j,k}/\Lambda^*_{i+3/4,j,k}, & \text{on } Q^*_{i+3/4,j,k} \\ 0, & \text{otherwise} \end{cases} \tag{12}$$

where now

$$\Lambda^*_{i+1/4,j,k} = \int_0^1\int_0^1\int_{1/2}^1 \mathbf{u}_{i+1/4,j,k}\mathbf{X}_{i,j,k}J_{i,j,k}\,d\hat{x}d\hat{y}d\hat{z}$$

$$\Lambda^*_{i+3/4,j,k} = \int_0^1\int_0^1\int_0^{1/2} \mathbf{u}_{i+3/4,j,k}\mathbf{X}_{i+1,j,k}J_{i+1,j,k}\,d\hat{x}d\hat{y}d\hat{z}$$

and

$$\mathbf{u}_{i+1/4,j,k} = \frac{(\Delta x_{i+1/4,j,k}, \Delta y_{i+1/4,j,k}, \Delta z_{i+1/4,j,k})}{\Delta s^2_{i+1/4,j,k}}$$

$$\mathbf{u}_{i+3/4,j,k} = \frac{(\Delta x_{i+3/4,j,k}, \Delta y_{i+3/4,j,k}, \Delta z_{i+3/4,j,k})}{\Delta s^2_{i+3/4,j,k}}$$

and $\Delta s_{i+1/4,j,k} = (\Delta x^2_{i+1/4,j,k} + \Delta y^2_{i+1/4,j,k} + \Delta z^2_{i+1/4,j,k})^{1/2}$, $\Delta s_{i+3/4,j,k} = (\Delta x^2_{i+3/4,j,k} + \Delta y^2_{i+3/4,j,k} + \Delta z^2_{i+3/4,j,k})^{1/2}$. Here, $(\Delta x_{i+1/4,j,k}, \Delta y_{i+1/4,j,k}, \Delta z_{i+1/4,j,k})$ is the vector from the physical centroid of cell $Q_{i,j,k}$ to the center of face $F_{i+1/2,j,k}$; $(\Delta x_{i+3/4,j,k}, \Delta y_{i+3/4,j,k}, \Delta z_{i+3/4,j,k})$ goes similarly from $F_{i+1/2,j,k}$ to $Q_{i+1,j,k}$. When applied to the left-hand side of (3), this test function gives the result

$$\begin{aligned}
&\int_{Q^*_{i+1/2,j,k}} \nabla p\cdot\mathbf{w}^*_{i+1/2,j,k}\,dxdydz \\
&= \frac{1}{\Lambda^*_{i+1/4,j,k}}\int_{Q^*_{i+1/4,j,k}} \nabla p\cdot\mathbf{X}_{i,j,k}\,dxdydz \\
&\quad + \frac{1}{\Lambda^*_{i+3/4,j,k}}\int_{Q^*_{i+3/4,j,k}} \nabla p\cdot\mathbf{X}_{i+1,j,k}\,dxdydz \\
&= \frac{1}{\Lambda^*_{i+1/4,j,k}}\int_0^1\int_0^1\int_{1/2}^1 \nabla p\cdot\mathbf{X}_{i,j,k}J_{i,j,k}\,d\hat{x}d\hat{y}d\hat{z} \\
&\quad + \frac{1}{\Lambda^*_{i+3/4,j,k}}\int_0^1\int_0^1\int_0^{1/2} \nabla p\cdot\mathbf{X}_{i+1,j,k}J_{i+1,j,k}\,d\hat{x}d\hat{y}d\hat{z} \\
&\approx p_{i+1,j,k} - p_{i,j,k}
\end{aligned} \tag{13}$$

The last result follows from the approximation that

$$-\frac{\partial p}{\partial (e_{\mathbf{u}})_{i+1/4,j,k}} \approx (p_{i,j,k} - p_{i+1/2,j,k})\,|\mathbf{u}_{i+1/4,j,k}|, \quad (x,y,z) \in Q^*_{i+1/4,j,k}$$

$$-\frac{\partial p}{\partial (e_{\mathbf{u}})_{i+3/4,j,k}} \approx (p_{i+1/2,j,k} - p_{i+1,j,k})\,|\mathbf{u}_{i+3/4,j,k}|, \quad (x,y,z) \in Q^*_{i+3/4,j,k}$$

where $e_{\mathbf{u}}$ is the unit vector $\mathbf{u}/|\mathbf{u}|$. That is, the pressure variation is assumed to be piecewise linear in physical space Q. However, this procedure does not insure that each piecewise linear approximation in the logical x, y and z directions is compatible with a constant ∇p. Because this test function represents a modification of the CJMR test function, it will be referred to as the MCJMR function.

Recently, Garanzha and Konshin (1999) have proposed a simple variant of the test function; their suggested form is

$$\mathbf{w}^{**}_{i+1/2,j,k} = \begin{cases} \mathbf{X}_{i,j,k}/J_{i,j,k}, & \text{on } Q^*_{i+1/4,j,k} \\ \mathbf{X}_{i+1,j,k}/J_{i+1,j,k}, & \text{on } Q^*_{i+3/4,j,k} \\ 0, & \text{otherwise} \end{cases} \tag{14}$$

This test function shall be subsequently referred to as the GK function. When applied to the left hand side of (3), this function yields

$$\begin{aligned}
&\int_{Q^*_{i+1/2,j,k}} \nabla p \cdot \mathbf{w}^{**}_{i+1/2,j,k}\, dxdydz \\
&= \int_{Q^*_{i+1/4,j,k}} \frac{\nabla p \cdot \mathbf{X}_{i,j,k}}{J_{i,j,k}}\, dxdydz \\
&\quad + \int_{Q^*_{i+3/4,j,k}} \frac{\nabla p \cdot \mathbf{X}_{i+1,j,k}}{J_{i+1,j,k}}\, dxdydz \\
&= \int_0^1 \int_0^1 \int_{1/2}^1 \nabla p \cdot \mathbf{X}_{i,j,k}\, d\hat{x}d\hat{y}d\hat{z} \\
&\quad + \int_0^1 \int_0^1 \int_0^{1/2} \nabla p \cdot \mathbf{X}_{i+1,j,k}\, d\hat{x}d\hat{y}d\hat{z} \\
&= \int_0^1 \int_0^1 \int_{1/2}^1 \frac{\partial p}{\partial \hat{x}}|_{Q^*_{i+1/4,j,k}}\, d\hat{x}d\hat{y}d\hat{z} \\
&\quad + \int_0^1 \int_0^1 \int_0^{1/2} \frac{\partial p}{\partial \hat{x}}|_{Q^*_{i+3/4,j,k}}\, d\hat{x}d\hat{y}d\hat{z} \\
&= \int_0^1 \int_0^1 \left(p|_{\hat{x}=1} - p|_{\hat{x}=1/2}\right)|_{Q^*_{i+1/4,j,k}}\, d\hat{y}d\hat{z} \\
&\quad + \int_0^1 \int_0^1 \left(p|_{\hat{x}=1/2} - p|_{\hat{x}=0}\right)|_{Q^*_{i+3/4,j,k}}\, d\hat{y}d\hat{z} \\
&= \int_0^1 \int_0^1 p|_{\hat{x}=1/2}\, d\hat{y}d\hat{z}|_{Q^*_{i+3/4,j,k}} \\
&\quad - \int_0^1 \int_0^1 p|_{\hat{x}=1/2}\, d\hat{y}d\hat{z}|_{Q^*_{i+1/4,j,k}} \\
&\approx p_{i+1,j,k} - p_{i,j,k}
\end{aligned} \tag{15}$$

Here, the major approximation is that the integral of the pressure over the center section in reference space is approximately equivalent to the average pressure. In the presence of a uniform flow field and in two dimensions, this approximation is exact even for an irregular grid; in three dimensions, even in the presence of a uniform flow field, some error will be introduced when an irregular grid is used to discretize the domain. Overall, this test function is the least restrictive as far as assumptions required for eliminating the pressure on intermediate faces.

Over the straddling control volume $Q^*_{i+1/2,j,k}$ the specific discharge is again approximated as a linear combination of fluxes and shape functions $(7a)$-$(7f)$. Allowing $\hat{\mathbf{q}}$ to be this approximation, then at any point in $Q^*_{i+1/2,j,k}$

$$\begin{aligned}
\hat{\mathbf{q}} &= f_{i+1/2,j,k}\left(\mathbf{v}_{i,j,k;1/2,0,0} + \mathbf{v}_{i+1,j,k;-1/2,0,0}\right) \\
&\quad + f_{i-1/2,j,k}\mathbf{v}_{i,j,k;-1/2,0,0} + f_{i+3/2,j,k}\mathbf{v}_{i+1,j,k;1/2,0,0} \\
&\quad + f_{i,j+1/2,k}\mathbf{v}_{i,j,k;0,1/2,0} + f_{i,j-1/2,k}\mathbf{v}_{i,j,k;0,-1/2,0} \\
&\quad + f_{i,j,k+1/2}\mathbf{v}_{i,j,k;0,0,1/2} + f_{i,j,k-1/2}\mathbf{v}_{i,j,k;0,0,-1/2} \\
&\quad + f_{i+1,j+1/2,k}\mathbf{v}_{i+1,j,k;0,1/2,0} \\
&\quad + f_{i+1,j-1/2,k}\mathbf{v}_{i+1,j,k;0,-1/2,0} \\
&\quad + f_{i+1,j,k+1/2}\mathbf{v}_{i+1,j,k;0,0,1/2} \\
&\quad + f_{i+1,j,k-1/2}\mathbf{v}_{i+1,j,k;0,0,-1/2}
\end{aligned} \tag{16}$$

Assuming that any of the above forms can be used as a test function, then a discrete form for the Darcy relation becomes

$$p_{i+1,j,k} - p_{i,j,k} = -\mu \int_{Q^*_{i+1/2,j,k}} \left(\mathbf{K}^{-1}\hat{\mathbf{q}}\right) \cdot \mathbf{w}\, dxdydz \tag{17}$$

where **w** can be any of the above test functions. Completion of the indicated integrations in (17) results in a set of coefficients relating the bulk fluxes on the various faces of $Q_{i,j,k}$ and $Q_{i+1,j,k}$ to the difference in pressures at the cell centers (at $\hat{x} = 1/2$, $\hat{y} = 1/2$, $\hat{z} = 1/2$ in each cell). This method is applied to all interior faces of the domain; thus a discrete Darcy relation is formed for every interior face. These relations and the discrete continuity equation (9), applied

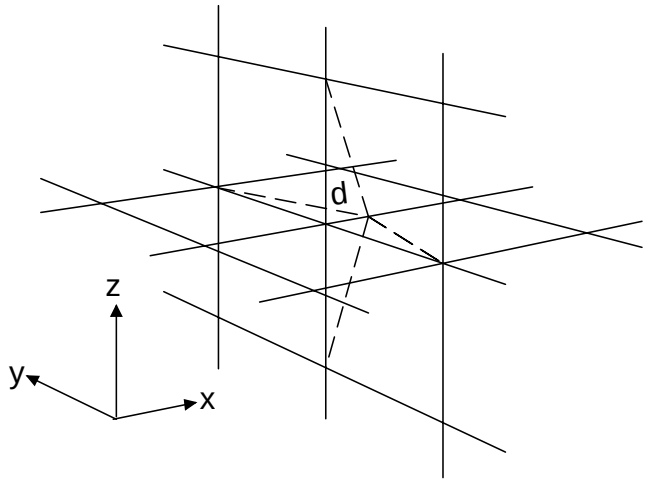

Figure 3: Method by which distortion is introduced into an otherwise orthogonal grid consisting of $4 \times 4 \times 4$ cells; vertex at center of domain is displaced into neighboring cells by distance d.

to every cell within the domain, form the sets of equations which are the basis of the CVMFE method. In applications to irregular grids, this system of equations is non-symmetric; otherwise, it is similar if not identical in structure to equations that result from other mixed-method techniques. The Schur complement (Dougherty 1990) was used to solve these equations for the test problems presented herein.

5 THREE-DIMENSIONAL, UNIFORM FLOW TESTS

In this section, the effect of grid distortion on the discrete L^2 norm of the velocity error is briefly investigated. Simulations with the CVMFE method of 2-D uniform flow on irregular grids give the result that the fluxes on the internal faces of the grid are estimated essentially exactly when the GK test function is used; this result is in agreement with the work of Garanzha and Konshin (1999). As there is always some error associated with simulations using the CJMR or MCJMR test functions, our 2-D results always indicated that the GK test function is superior for simulating uniform flow on irregular grids. In three dimensions, simulations of uniform flow on irregular grids with the GK test function do not produce exact flux results on interior faces. We attempt to quantify the difference in performance between the three test functions using a simple grid-distortion test; in particular, grid distortion which results in cells with non-planar faces is considered. A test module was created by considering uniform flow through a 3-D domain consisting of $4 \times 4 \times 4$ cells in which all the cell edges are equidimensional and orthogonal. As depicted in Figure 3, a distortion in the otherwise regular discretization is produced by moving the vertex at the center of the grid along the adjacent cell edge boundary in the x direction; the four faces adjoining this vertex, which were originally perpendicular to the x direction, become increasingly non-planar as the offset d is increased. Constant flux boundary conditions are imposed at both the upstream ($x = 0$) and downstream ($x = 4$) ends of the domain so as to ensure a uniform flow field. The numerical model produces essentially exact flux estimates for all interior faces of the discretized domain when $d = 0$; that is, on orthogonal grids all three test functions are equivalent and produce, for uniform flow, exact simulations. As d increases, errors in the numerical flux estimates are to be found on all faces in the domain, but are greatest near the distortion. As flow is uniform and in the x direction, the normal fluxes across all faces are easily calculated by projecting cell facial areas onto the upstream face of the domain. The exact fluxes were compared with the calculated fluxes using L^2 norms. More precisely, the mean normal velocity error for each face was obtained by dividing the difference of these fluxes by the facial area; then a root-mean-square of these errors, weighted by the relative volume of the control volume associated with each face, was calculated. This is essentially an L^2 norm of the velocity error, normalized by the L^2 norm of a unit vector.

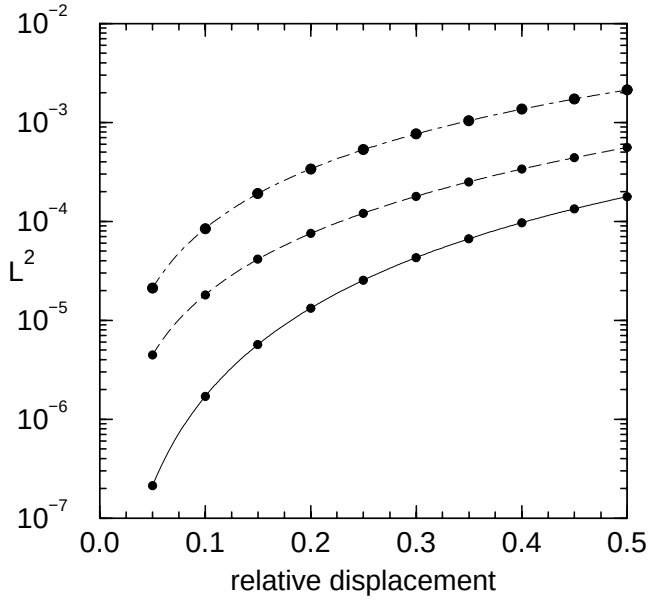

Figure 4: L^2 norm results for various test functions from the uniform flow, simply distorted grid experiment. Solid line: GK test function; dashed line: MCJMR test function; dashed and dotted line: CJMR test function.

Figure 4 is a depiction of the L^2 norm results as a function of the relative displacement d for the three test functions given previously. From these results, the performance of the algorithm with the GK test function is shown to be significantly superior to that of the CJMR or MCJMR test functions; the CVMFE method

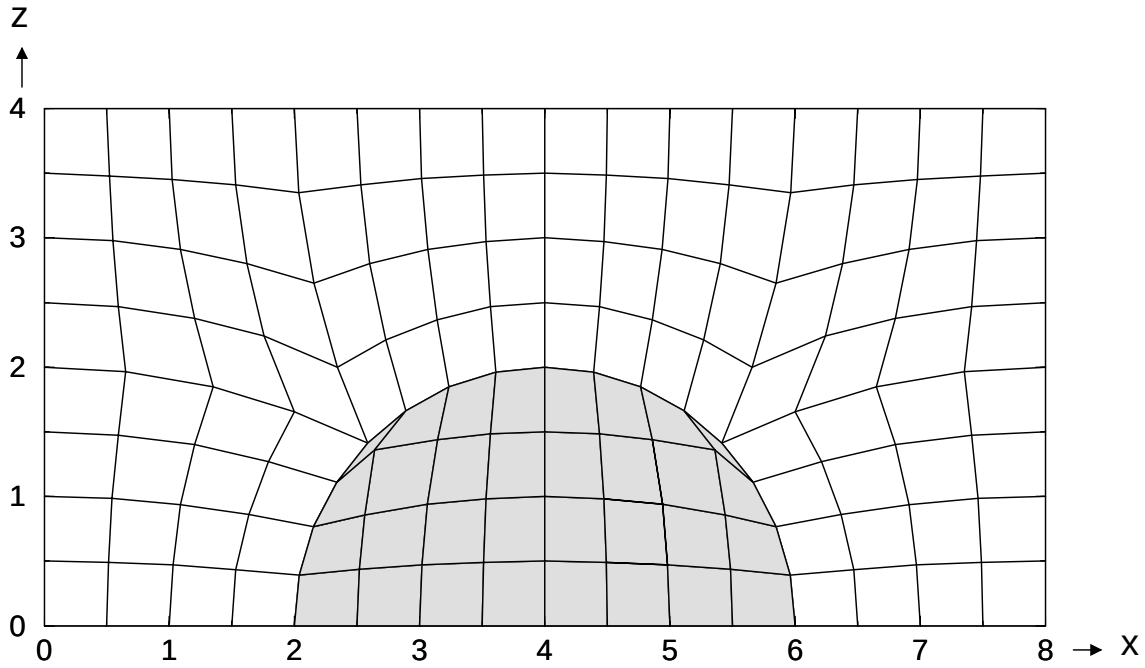

Figure 5: Core discretization for disk-shaped heterogeneity problem. Shaded area represents region of conductivity K_1; remaining domain has conductivity K_2. Flow is largely from left to right.

with the GK test function outperforms the CJMR test function by an order of magnitude. Other 3-D simulations of uniform flow in the presence of an irregular grid that we have experimented with also indicated the superiority of the GK test function; however, the difference in performance of the various test functions may not be as great. For example, simulations of uniform flow have been performed with grids consisting of $4 \times 4 \times 4$ cells in which all the internal cell faces are planar but have limited random orientations; in these simulations, the exterior faces of the simulation domain were planar and orthogonal. For this particular example, the CVMFE method with the GK, MCJMR and CJMR test functions give L^2 norms of 1.04×10^{-3}, 1.27×10^{-3} and 1.46×10^{-3}, respectively. However, that none of these 3-D simulations of uniform flow on irregular grids with random faces are exact, or even nearly so, causes us to suspect that that the aforementioned problems with the 3-D shape functions may be affecting these results. If this is the case, then these L^2 norm results may largely reflect the difficulty of using shape functions $(7a)$-$(7f)$ as velocity basis functions for 3-D simulations. Thus, for other forms of grid irregularity we can only say, at this time, that using the GK test function in the CVMFE method appears to be marginally superior for simulating 3-D uniform flow, but this marginal performance may in large part be a result of using shape functions $(7a)$-$(7f)$ in the CVMFE algorithm. An example of an essentially exact simulation for 2-D, uniform flow is given in the next section.

6 TWO-DIMENSIONAL, NONUNIFORM FLOW TEST

In order to examine the performance of the various test functions under nonuniform flow conditions, a 2-D problem consisting of a disk-shaped heterogeneity embedded in an otherwise uniform medium was selected (Figure 5). In this test problem, nonuniform flow is produced in an otherwise uniform flow field by altering the hydraulic conductivity in the embedded, disk-shaped heterogeneity so that it contrasts with the hydraulic conductivity of the remainder of the domain. Here, the hydraulic conductivity K_1 of the embedded, disk-shaped medium is assumed to be equal to or greater than the hydraulic conductivity K_2 of the embedding medium. When this heterogeneous geometry is posed for an infinite domain, an analytical solution is available that gives pressure as a function of space and the contrast in hydraulic conductivity between the disk-shaped heterogeneity and the remainder of the domain (Carslaw & Jaeger 1959); in this case, flow is assumed to be uniform at an infinite distance from the heterogeneity. As depicted in Figure 5, this heterogeneous geometry is relatively easy to discretize for a finite domain; here, it is assumed that, in the absence of a contrast in hydraulic conductivity, flow would be uniform and from left to right in the x direction. For simulation purposes, the core discretization depicted in this figure was extended by adding four more layers of cells at the $x = 0$, $x = 8$ and $z = 4$ boundaries; these cells were all orthogonal with the dimensions $1/2 \times 1/2$. The purpose of these additional cell layers was to shift the boundary conditions farther from the disk-shaped heterogene-

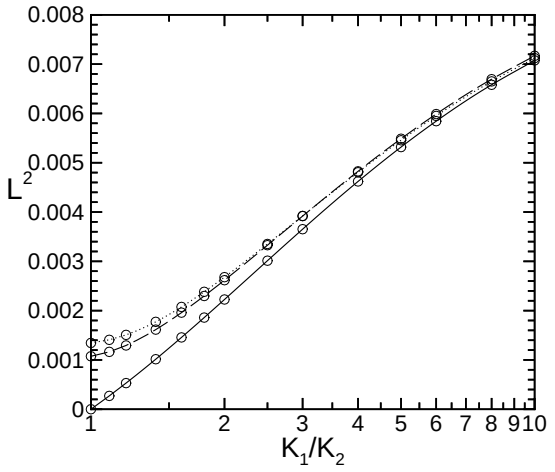

Figure 6: L^2 norm results for various test functions from the 2-D, nonuniform flow experiment. Solid line: GK test function; dashed line: MCJMR test function; dotted line: CJMR test function.

ity and thus minimize their influence on the resulting simulations. Flux boundary conditions were imposed at $x = -2$, $x = 10$ and $z = 6$; these boundary conditions were extracted from the analytical solution by integrating the normal velocity component, as obtained from the analytical solution, over the exterior cell faces on these boundaries. For each different hydraulic conductivity contrast, it was necessary to generate a new flux boundary condition. Facially averaged velocities from the analytical solution were used as exact velocities in calculating the L^2 norms; the L^2 norms were calculated only over the irregular faces of the core discretization shown in Figure 5.

The performance of the various test functions for this test case, as described by the L^2 norm, is depicted in Figure 6. Here, the L^2 norm results are presented as a function of the ratio K_1/K_2, representing the contrast in hydraulic conductivity, which was allowed to vary from unity (no contrast) to ten (high contrast). When $K_1/K_2 = 1$, the L^2 norm for the simulations using the GK test function is null, while the simulations with the CJMR or MCJMR test functions are finite and moderately significant; this then is an example of 2-D uniform flow simulation where the results from using the GK test function are exact. However, the difference in L^2 norms for simulations with these various test functions decreases rather rapidly as the ratio K_1/K_2 increases; when $K_1/K_2 = 10$, there is little difference between the various L^2 norm results. Apparently, as nonuniform flow begins to dominate the simulation, it becomes more difficult for the shape functions to locally approximate the velocity field and the simulation error is increased. Thus, when flow is strongly nonuniform, the approximation associated with the shape functions $(7a)$-$(7f)$ appears to be a greater source of error than that associated with the test function.

7 CONCLUDING REMARKS

In general, results given here indicate that the GK test function proposed by Garanzha and Konshin (1999) produces the best overall results. While it is possible to simulate exactly uniform flow on two-dimensional, irregular grids using the GK test function, we have not been able to repeat this feat in three dimensions. This may be the result of a poor scaling of the shape functions between two and three dimensions, but may also result, in part, from a difference in the averaging properties of the test function. That is, while the GK test function in two dimensions gives a true average of the pressure, the average is weighted in three dimensions. We suspect, however, that deficiencies in the shape functions $(7a)$-$(7f)$ are a more significant factor in the inability of the current CVMFE algorithm to exactly simulate 3-D uniform flow on irregular grids. In the simulation of a highly nonuniform, two-dimensional flow field, the superiority of the GK test function is less evident; this may simply be the result of using a rather coarse grid for the simulation in this test. The GK test function does appear to perform better in simulations involving non-planar faces on cells. Non-planar faces are expected to be a common feature of 3-D, irregular grids; thus, the GK test function is likely to be an important factor in extending the CVMFE methology to three dimensions.

ACKNOWLEDGMENTS: The research of the second author was supported in part by National Science Foundation Grant No. DMS-9706866 and Army Research Office Grant No. 37119-GS-AAS.

REFERENCES

Cai, Z., Jones, J., McCormick, S., & Russell, T. (1997). Control volume mixed finite element methods. *Computational Geosciences 1*, 289–315.

Carslaw, H. & Jaeger, J. (1959). *Conduction of Heat in Solids*. Oxford: Oxford University Press.

Dougherty, D. (1990). PCG solutions of flow problems in random porous media using mixed finite elements. *Adv. Water Resources 13*(1), 2–11.

Durlofsky, L. (1994). Accuracy of mixed and control volume finite element approximations to Darcy velocity and related quantities. *Water Resour. Res. 30*(4), 965–973.

Garanzha, V. & Konshin, V. (1999). Approximation schemes and discrete well models for the numerical simulation of the 2-d non-Darcy fluid flows in porous media. Comm. on appl. math., Computer Centre, Russian Academy of Science, Moscow.

Hildebrand, F. (1962). *Advanced Calculus for Applications*. Englewood Cliffs: Printice-Hall.